

1 **GPU-HADVPPM V1.0: A high-efficiency parallel GPU design of**
2 **the piecewise parabolic method (PPM) for horizontal advection**
3 **in an air quality model (CAMx V6.10)**

4 **Kai Cao¹, Qizhong Wu¹, Lingling Wang², Nan Wang², Huaqiong Cheng¹, Xiao**
5 **Tang³, Dongqing Li¹, and Lanning Wang¹**

6 ¹College of Global Change and Earth System Science, Beijing Normal University,
7 Beijing 100875, China

8 ²Henan Ecological Environmental Monitoring Centre and Safety Center, Henan Key
9 Laboratory of Environmental Monitoring Technology, Zhengzhou 450008, China

10 ³State Key Laboratory of Atmospheric Boundary Layer Physics and Atmospheric
11 Chemistry, Institute of Atmospheric Physics, Chinese Academy of Science, Beijing
12 100029, China

13
14 **Correspondence to:** Qizhong Wu (wqizhong@bnu.edu.cn); Lingling Wang
15 (928216422@qq.com); Lanning Wang (wangln@bnu.edu.cn)
16

17 **Abstract.** With semiconductor technology gradually approaching its physical and
18 thermal limits, graphics processing units (GPUs) are becoming an attractive solution
19 for many scientific applications due to their high performance. This paper presents an
20 application of GPU accelerators in an air quality model. We demonstrate an approach
21 that runs a PPM solver of horizontal advection (HADVPPM) for the air quality model
22 CAMx on GPU clusters. Specifically, we first convert the HADVPPM to a new
23 Compute Unified Device Architecture C (CUDA C) code to make it computable on the
24 GPU (GPU-HADVPPM). Then, a series of optimization measures are taken, including
25 reducing the CPU-GPU communication frequency, increasing the data size
26 computation on the GPU, optimizing the GPU memory access, and using thread and
27 block indices to improve the overall computing performance of the CAMx model
28 coupled with GPU-HADVPPM (named the CAMx-CUDA model). Finally, a
29 heterogeneous, hybrid programming paradigm is presented and utilized with the GPU-
30 HADVPPM on the GPU clusters with a message passing interface (MPI) and CUDA.
31 The offline experimental results show that running GPU-HADVPPM on one NVIDIA
32 Tesla K40m and an NVIDIA Tesla V100 GPU can achieve up to a 845.4x and 1113.6x

删除的内容: efficient

批注 [A2]: Your document was edited for correct English language, grammar, punctuation, and phrasing. In addition, we have made some changes to ensure consistency throughout the document. These changes are based on our extensive knowledge of what journals typically require. If you would like more details, please contact our Support team.

删除的内容: Piecewise Parabolic Method

删除的内容: Graphics

删除的内容: unit (GPU) is

删除的内容: in

删除的内容: endeavor to

删除的内容: size of

删除的内容: ,

删除的内容: in order

删除的内容: as

删除的内容: Message Passing Interface

删除的内容: Offline

删除的内容: experiment

46 acceleration. By implementing a series of optimization schemes, the CAMx-CUDA
47 model results in a 29.0x and 128.4x improvement in computational efficiency by using
48 a GPU accelerator card on a K40m and V100 cluster, respectively. In terms of the
49 single-module computational efficiency of GPU-HADVPPM, it can achieve 1.3x and
50 18.8x speedup on an NVIDIA Tesla K40m GPU and NVIDA Tesla V100 GPU,
51 respectively. The multi-GPU acceleration algorithm enables a 4.5x speedup with 8 CPU
52 cores and 8 GPU accelerators on a V100 cluster.

删除的内容: resulted

53 1. Introduction

54 Since the introduction of personal computers in the late 1980s, the computer and
55 mobile device industry has created a flourishing worldwide market (Bleichrodt et al.,
56 2012). In recent years, improvements of the central processing unit (CPU) performance
57 has been limited by its heat dissipation, and the applicability of Moore's Law has
58 flattened. A common trend in high-performance computing today is the utilization of
59 hardware accelerators, which execute codes rich in data parallelism, to form high-
60 performance heterogeneous systems. GPUs are widely used as accelerators due to their
61 high peak performances. In the top ten supercomputing list released in December 2022
62 (<https://www.top500.org/lists/top500/list/2022/11/>, last access: 19 December 2022),
63 there were seven heterogeneous supercomputing platforms built with CPU processors
64 and GPU accelerators, of which the top one, Frontier at the Oak Ridge National
65 Laboratory, uses AMD's third-generation EPYC CPU and AMD's Instinct MI250X
66 GPU, and its computing performance reaches exascale levels (10^{18} calculations per
67 second) for the first time ([https://www.amd.com/en/press-releases/2022-05-30-world-
68 s-first-exascale-supercomputer-powered-amd-epyc-processors-and-amd](https://www.amd.com/en/press-releases/2022-05-30-world-s-first-exascale-supercomputer-powered-amd-epyc-processors-and-amd), last access:
69 19 December 2022). Such a powerful computing performance of the heterogeneous
70 system not only injects new vitality into high-performance computing, but also
71 generates new solutions for improving the performance of geoscience numerical
72 models.

删除的内容: the

删除的内容: computer

删除的内容: been one

删除的内容: of the most

删除的内容: markets all over the world

删除的内容: the

删除的内容: of the performance of the C

删除的内容: Processing

删除的内容: Unit

删除的内容: is

删除的内容: development

删除的内容: that

删除的内容: system

删除的内容: offered

删除的内容: are

删除的内容:

删除的内容: Exascale

删除的内容: ,

删除的内容: provides

删除的内容: in geoscience

94 The GPU has proven successful in weather models such as the nonhydrostatic
 95 icosahedral model (NIM; Govett et al., 2017), global/regional assimilation and
 96 prediction system (GRAPES; Xiao et al., 2022), weather research and forecasting
 97 model (WRF; Huang et al., 2011; Huang et al., 2012; Mielikainen et al., 2012a;
 98 Mielikainen et al., 2012b; Mielikainen et al., 2013a; Mielikainen et al., 2013b; Price et
 99 al., 2014; Huang et al., 2015), ocean models such as the LASG/IAP climate system
 100 ocean model (LICOM; Jiang et al., 2019; Wang et al., 2021a) and Princeton ocean
 101 model (POM; Xu et al., 2015), and earth system model of the Chinese Academy of
 102 Sciences (CAS-ESM; Wang et al., 2016; Wang et al., 2021b).

删除的内容: Non-Hydrostatic...he N...onhydrostatic
 Icosahedral ...cosahedral Model ...odel (NIM; Govett et al., 2017),
 Global...lobal/Regional ...egional Assimilation ...ssimilation and
 Prediction ...rediction System ...ystem (GRAPES; Xiao et al., 2022),
 and W...eather Research ...earch and Forecasting ...orecasting
 model (WRF; Huang et al., 2011; Huang et al., 2012; Mielikainen et
 al., 2012a; Mielikainen et al., 2012b; Mielikainen et al., 2013a ...
 Mielikainen et al., 2013b; Price et al., 2014; Huang et al., 2015),
 ocean models such as the LASG/IAP Climate ...limate
 System ...ystem Ocean ...cean Model ...odel (LICOM; Jiang et al.,
 2019; Wang et al., 2021a) and Princeton Ocean ...cean Model ...odel
 (POM; Xu et al., 2015),...and the...Earth ...arth System ...ystem
 Model ...odel of the Chinese Academy of Sciences (CAS-ESM;
 Wang et al., 2016; Wang et al., 2021b). ... [1]

103 Govett et al. (2017) used open accelerator (OpenACC) directives to port the
 104 dynamics of NIM to the GPU and achieved a 2.5x acceleration. Additionally, using
 105 OpenACC directives, Xiao et al. (2022) ported the PRM (piecewise rational method)
 106 scalar advection scheme in GRAPES to the GPU, achieving up to 3.51x faster results
 107 than 32 CPU cores. In terms of the most widely used WRF, several parameterization
 108 schemes, such as the RRTMG_LW scheme (Price et al., 2014), 5-layer thermal
 109 diffusion scheme (Huang et al., 2015), Eta Ferrier cloud microphysics scheme (Huang
 110 et al., 2012), Goddard shortwave scheme (Mielikainen et al., 2012a), Kessler cloud
 111 microphysics scheme (Mielikainen et al., 2013b), SBU-YLIN scheme (Mielikainen et
 112 al., 2012b), WMS5 scheme (Huang et al., 2011), and WMS6 scheme (Mielikainen et al.,
 113 2013a), have been ported heterogeneously using CUDA C and achieved 37x~896x
 114 acceleration results. LICOM has conducted heterogeneous porting using OpenACC
 115 (Jiang et al., 2019) and used heterogeneous-compute interface for portability C (HIP C)
 116 technologies, and achieved up to a 6.6x and 42x acceleration, respectively (Wang et al.,
 117 2021a). For the Princeton ocean model, Xu et al. (2015) use CUDA C to conduct
 118 heterogeneous porting and optimization, and the performance of gpu-POM v1.0 on four
 119 GPUs is comparable to that on the 408 standard Intel Xeon X5670 CPU cores. In terms
 120 of climate system models, Wang et al. (2016) and Wang et al. (2021b) used CUDA
 121 Fortran and CUDA C to conduct heterogeneous porting of the RRTMG SW and
 122 RRTMG_LW schemes of the atmospheric component model of the CAS-ESM earth

删除的内容: ... (2017) used Open ...pen Accelerator ...ccelerator
 (OpenACC) directives to port the dynamics of NIM to the GPU and
 achieved a 2.5x acceleration. Also...ditionally, using OpenACC
 directives, Xiao et al.,... (2022) ported the PRM (Piecewise Rational
 Method...iecewise rational method) scalar advection scheme in
 the ...RAPES to the GPU, achieving up to 3.51x faster results than
 32 CPU cores. In terms of the most widely used WRF, several
 parameterization schemes, such as the RRTMG_LW scheme (Price et
 al., 2014), 5-layer thermal diffusion scheme (Huang et al., 2015), Eta
 Ferrier Cloud ...loud Microphysics ...icrophysics scheme (Huang et
 al., 2012), Goddard Shortwave ...hortwave scheme (Mielikainen et
 al., 2012a), Kessler cloud microphysics scheme (Mielikainen et al.,
 2013b), SBU-YLIN scheme (Mielikainen et al., 2012b), WMS5
 scheme (Huang et al., 2011),...and WMS6 scheme (Mielikainen et
 al., 2013a), etc.,...ave been ported heterogeneously using CUDA C
 and achieved 37x~896x acceleration results. The...LICOM has
 carried out...onducted heterogeneous porting using OpenACC (Jiang
 et al., 2019) and used Heterogeneous...eterogeneous-compute
 Interface for Portability ...nterface for portability C (HIP C)
 technologies,... and achieved up to a 6.6x and 42x acceleration,
 respectively (Wang et al., 2021a). For the Princeton Ocean ...cean
 Model...odel, Xu et al.,... (2015) use CUDA C to carry out...onduct
 heterogeneous porting and optimization, and the performance of gpu-
 POM v1.0 on four GPUs is comparable to that on the 408 standard
 Intel Xeon X5670 CPU cores. In terms of the...climate system
 models, Wang et al.,... (2016) and Wang et al.,... (2021b) used CUDA
 Fortran and CUDA C to carry out...onduct heterogeneous porting of
 the RRTMG_SW and RRTMG_LW scheme ... [2]

216 system model and achieved a 38.88x and 77.78x acceleration, respectively.

217 Programming a GPU accelerator can be a difficult and error-prone process that
218 requires specially designed programming methods. There are three widely used
219 methods for porting programs to GPUs, as described above. The first method uses the
220 OpenACC directive (<https://www.openacc.org/>, last access: 19 December 2022), which
221 provides a set of high-level directives that enable C/C++ and Fortran programmers to
222 utilize accelerators. The second method uses CUDA Fortran. CUDA Fortran is a
223 software compiler that was codeveloped by the Portland Group (PGI) and NVIDIA,
224 and is a tool chain for building performance-optimized GPU-accelerated Fortran
225 applications targeting the NVIDIA GPU platform ([https://developer.nvidia.com/cuda-
226 fortran](https://developer.nvidia.com/cuda-fortran), last access: 19 December 2022). Using CUDA C involves rewriting the entire
227 program using the standard C programming language and low-level CUDA subroutines
228 (<https://developer.nvidia.com/cuda-toolkit>, last access: 19 December 2022) to support
229 the NVIDIA GPU accelerator. Compared to the other two technologies, the CUDA C
230 porting scheme is the most complex, but it has the highest computational performance
231 (Mielikainen et al., 2012b; Wahib and Maruyama, 2013; Xu et al., 2015).

232 Air quality models are critical for understanding how the chemistry and
233 composition of the atmosphere may change throughout the 21st century, as well as for
234 preparing adaptive responses or developing mitigation strategies. Because air quality
235 models need to take into account the complex physicochemical processes that occur in
236 the atmosphere of anthropogenic and natural emissions, simulations are
237 computationally expensive. Compared to other geoscientific numerical models, few
238 studies have conducted a heterogeneous porting of air quality models. In this study, the
239 CUDA C scheme, implemented in this paper, conducted a hotspot module porting of
240 CAMx to improve the computation efficiency.

删除的内容: ,

删除的内容: a

删除的内容: hard

删除的内容: programing

删除的内容: , there

删除的内容: program

删除的内容: which co-developed

删除的内容: ,

删除的内容:

删除的内容:

删除的内容: ,

删除的内容: its computational performance is the highest

删除的内容:

删除的内容: to

删除的内容: atmospheric

删除的内容: over

删除的内容: naturally

删除的内容: the

删除的内容: research

删除的内容: carried out

删除的内容: was

删除的内容: to carry out the

删除的内容: attempt

删除的内容: in order

265 **2. The CAMx model and experiments**

266 **2.1. Model description**

267 The CAMx model is a state-of-the air quality model developed by Ramboll
268 Environ (<https://www.camx.com/>, last access: 19 December 2022). CAMx version 6.10
269 (CAMx V6.10; ENVIRON, 2014) is chosen in this study; it simulates the emission,
270 dispersion, chemical reaction, and removal of pollutants by marching the Eulerian
271 continuity equation forward in time for each chemical species on a system of nested
272 three-dimensional grids. The Eulerian continuity equation is expressed mathematically
273 in terrain-following height coordinates as Formula (1):

$$\begin{aligned} 274 \quad \frac{\partial c_i}{\partial t} = & -\nabla_H \cdot V_H c_i + \left[\frac{\partial(c_i \eta)}{\partial z} - c_i \frac{\partial^2 h}{\partial z \partial t} \right] + \nabla \cdot \rho K \nabla (c_i / \rho) \\ 275 \quad & + \left. \frac{\partial c_i}{\partial t} \right|_{Emission} + \left. \frac{\partial c_i}{\partial t} \right|_{Chemistry} + \left. \frac{\partial c_i}{\partial t} \right|_{Removal} \end{aligned} \quad (1)$$

$$276 \quad \nabla_H \cdot \rho V_H = \frac{m^2}{A_{yz}} \frac{\partial}{\partial x} \left(\frac{u A_{yz} \rho}{m} \right) + \frac{m^2}{A_{xz}} \frac{\partial}{\partial y} \left(\frac{v A_{xz} \rho}{m} \right) \quad (2)$$

277 The first term on the right-hand side represents horizontal advection. In numerical
278 methods, the horizontal advection equation (described in Formula (2)) is performed
279 using the area preserving flux-form advection solver of the piecewise parabolic method
280 (PPM) of Colella and Woodward (1984) as implemented by Odman and Ingram (1996).
281 The PPM horizontal advection solution (HADVPPM) was incorporated into the CAMx
282 model because it provides higher order accuracy with minimal numerical diffusion.

283 In the Fortran code implementation of the HADVPPM scheme, the CAMx main
284 program calls the emistrns program, which mainly performs physical processes such as
285 emission, diffusion, advection and dry/wet deposition of pollutants. Then, the
286 horizontal advection program is invoked by the emistrns program to solve the
287 horizontal advection equation by using the HADVPPM scheme.

删除的内容: ,

删除的内容: ,

删除的内容: sforward

删除的内容: formula

删除的内容: the

删除的内容: equation of

删除的内容: formula

删除的内容: Piecewise Parabolic Method

删除的内容:

删除的内容: solution of

删除的内容:

删除的内容: the

删除的内容: And then

301 2.2. Benchmark performance experiments

302 The first porting step is to test the performance of the CAMx benchmark version
303 and identify the model's hotspots. On the Intel x86 CPU platform, we launch two
304 processes concurrently to run the CAMx, and take advantage of the Intel trace analyzer
305 collector (ITAC; [https://www.intel.com/content/www/us/en/docs/trace-analyzer-](https://www.intel.com/content/www/us/en/docs/trace-analyzer-collector/get-started-guide/2021-4/overview.html)
306 [collector/get-started-guide/2021-4/overview.html](https://www.intel.com/content/www/us/en/docs/trace-analyzer-collector/get-started-guide/2021-4/overview.html), last access: 19 December 2022) and
307 the Intel VTune profiler
308 (VTune; [https://www.intel.com/content/www/us/en/develop/documentation/vtune-](https://www.intel.com/content/www/us/en/develop/documentation/vtune-help/top.html)
309 [help/top.html](https://www.intel.com/content/www/us/en/develop/documentation/vtune-help/top.html), last access: 19 December 2022) performance analysis tools to collect
310 performance information during the CAMx operation.

311 The general MPI performance can be reported by the ITAC tool, and MPI load
312 balance information, computation and communication profiling of each process is
313 shown in Fig. 1a. During the running process of the CAMx model, Process 0 (P0)
314 spends 99.6% of the time on the MPI_Barrier function and only 0.4% of the time on
315 computation, while Process 1 (P1) spends 99.8% of its time computation and only 0.2%
316 of its time receiving messages from P0. It is apparent that the parallel design of the
317 CAMx model adopts the Master-Slave mode, and P0 is responsible for inputting and
318 outputting the data and calling the MPI_Barrier function to synchronize the process, so
319 there is a lot of MPI waiting time. The other processes are responsible for computation.

320 The VTune tool detects each module's runtime and the most time-consuming
321 functions on P1. As shown in Figure 1b, the top four time-consuming modules are
322 chemistry, diffusion, horizontal advection and vertical advection in the CAMx model.
323 In the above four modules, the top five most time-consuming programs are the ebrate,
324 hadvppm, tridiag, diffus and ebisolv programs, and the total runtime of P1 is 325.1
325 seconds. Top1 and Top2's most time-consuming programs take 49.4 and 35.6 seconds,
326 respectively.

327 By consideration, the hadvppm program was selected to conduct heterogeneous
328 porting for several reasons. First, the advection module is one of the air quality model's
329 compulsory modules, and is mainly used to simulate the transport process of air

删除的内容: step of the

删除的内容: of the model

删除的内容: Trace

删除的内容: A

删除的内容: Analyzer

删除的内容: Collector

删除的内容: Profiler

删除的内容:

删除的内容: as

删除的内容: indicated

删除的内容:

删除的内容: ,

删除的内容: ,

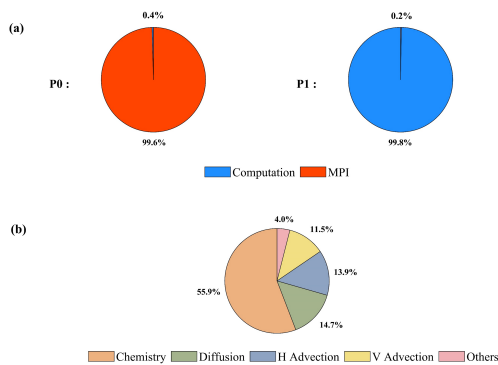
删除的内容: carry out

删除的内容: some

删除的内容: Firstly

删除的内容: of the air quality model, which

347 pollutants, additionally it is also a hotspot module detected by the Intel VTune tool. The
 348 typical air quality models, CAMx, CMAQ and NAQPMS, include advection modules
 349 and use the exact PPM advection solver. The heterogeneous version developed in this
 350 study can be directly applied to the above models. Furthermore, the weather model (e.g.,
 351 WRF) also contains an advection module, so this study's heterogeneous porting method
 352 and experience can be used for reference. Therefore, a GPU acceleration version of the
 353 HADVPPM scheme, namely, GPU-HADVPPM, is built to improve the CAMx
 354 performance.



355
 356 **Figure 1.** The computation performance of the modules in the CAMx model. (a) Computation and
 357 communication profiling of P0 and P1. (b) Overhead proportions of P1. The top four most time-
 358 consuming modules are chemistry, diffusion, horizontal advection and vertical advection.

360 2.3. Porting scheme introduction

361 The CAMx-CUDA heterogeneous scheme is shown in Figure 2. The second time-
 362 consuming hadvppm program in the CAMx model was selected to implement
 363 heterogeneous porting. To map the hadvppm program to the GPU, the Fortran code was
 364 converted to standard C code. Then, the CUDA programming language, which was
 365 tailor-made for NVIDIA, was added to convert the standard C code into CUDA C for

删除的内容: and

删除的内容: Then,

删除的内容: ,

批注 [A3]: Please note that we have not checked the text in this figure or any other figures that are not editable in Word. Please contact our support staff and provide text that can be directly modified in Microsoft Word or PowerPoint for all figure text that you would like revised.

删除的内容: ,

删除的内容: heterogeneous scheme of

删除的内容: the

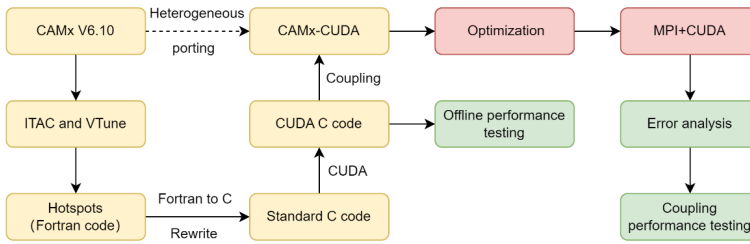
删除的内容: In order to

删除的内容: programing

374 data-parallel execution on the GPU, as GPU-HADVPPM. It prepared the input data for
 375 GPU-HADVPPM by constructing random numbers, and tested its offline performance
 376 on the GPU platform.

377 After coupling the GPU-HADVPPM to the CAMx model, the advection module
 378 code was optimized according to the characteristics of the GPU architecture to improve
 379 the overall computational efficiency on the CPU-GPU heterogeneous platform. Then,
 380 the multi-CPU core and multi-GPU card acceleration algorithm was adopted to improve
 381 the parallel extensibility of heterogeneous computing. Finally, the coupling
 382 performance test is implemented after verifying the different CAMx model simulation
 383 results.

删除的内容: And then



384
 385 **Figure 2.** Heterogeneous porting scheme of the CAMx-CUDA model.

386 2.4. Hardware components and software environment of the testing system

387 The experiments are conducted on two GPU clusters, K40m and V100. The
 388 hardware components and software environment of the two clusters are listed in Table
 389 1. The K40m cluster is equipped with two 2.5 GHz 16-core Intel Xeon E5-2682 v4
 390 CPU processors and one NVIDIA Tesla K40m GPU card on each node. The NVIDIA
 391 Tesla K40m GPU has 2880 CUDA cores with 12 GB of memory. The V100 cluster
 392 contains two 2.7 GHz 24-core Intel Xeon Platinum 8168 processors and eight NVIDIA
 393 Tesla V100 GPU cards with 5120 CUDA cores and 16 GB memory on each card.

删除的内容: .

删除的内容:

删除的内容: 5GHz

删除的内容: 12GB

删除的内容: 7GHz

删除的内容: 16GB

删除的内容:

394 **Table 1.** Configurations of GPU cluster.

Hardware components	
CPU	GPU

K40m cluster	Intel Xeon E5-2682 v4 CPU @2.5 GHz, 16 cores	NVIDIA Tesla K40m, 2880 CUDA cores, 12GB memory
V100 cluster	Intel Xeon Platinum 8168 CPU @2.7 GHz, 24 cores	NVIDIA Tesla V100, 5120 CUDA cores, 16GB memory
Software environment		
	Compiler and MPI	Programming Model
K40m cluster	Intel-2021.4.0	CUDA-10.2
V100 cluster	Intel-2019.1.144	CUDA-10.0

删除的内容: 5GHz

403 For Fortran and standard C programming, Intel Toolkit (including compiler and
 404 MPI library) version 2021.4.0 and version 2019.1.144 are employed for compiling on
 405 an Intel Xeon E4-2682 v4 CPU and Intel Xeon Platinum 8168 CPU, respectively. Then,
 406 CUDA version 10.2 and version 10.0 are employed on an NVIDIA Tesla K40m GPU
 407 and NVIDIA Tesla V100 GPU. CUDA (NVIDIA, 2020) is an extension of the C
 408 programming language that offers direct programming of the GPUs. In CUDA
 409 programming, a kernel is actually a subroutine that can be executed on the GPU. The
 410 underlying code in the kernel is divided into a series of threads, each with a unique "ID"
 411 number that simultaneously process different data through a single-instruction multiple-
 412 thread (SIMT) parallel mode. These threads are grouped into equal-sized thread blocks,
 413 which are organized into a grid.

删除的内容: Intel

删除的内容: And then

删除的内容: what is called

删除的内容: can

414 **3. Porting and optimization of the CAMx advection module on a heterogeneous** 415 **platform**

416 **3.1. Mapping the HADVPPM scheme to the GPU**

417 **3.1.1. Manual code translation from Fortran to standard C**

418 As the CAMx V6.10 code was written in Fortran 90, we rewrote the hadvppm
 419 program from Fortran to CUDA C. As an intermediate conversion step, we refactor the
 420 original Fortran code using standard C. During the refactoring, some of the
 421 considerations are listed in Table 2:

删除的内容: some

删除的内容: considerations

删除的内容: are

422 (1) The subroutine name refactored with standard C must be followed by an

431 underscore identifier, which can only be recognized when Fortran calls.

432 (2) In the Fortran language, the parameters are transferred by a memory address
 433 by default. In the case of mixed programming in Fortran and standard C, the parameters
 434 transferred by Fortran are processed by the pointer in standard C.

435 (3) Variable precision types defined in standard C must be strictly consistent with
 436 those in Fortran.

437 (4) Some built-in functions in Fortran are not available in standard C₂ and need to
 438 be defined in the standard C macro definitions.

439 (5) For multidimensional arrays, Fortran and standard C follow a column-major
 440 and row-major order, and in-memory read and write, respectively;

441 (6) Array subscripts in Fortran and standard C are indexed from any integer and 0,
 442 respectively.

443 **Table 2.** Some considerations during Fortran to C refactoring.

	Fortran code	C code
Function name	<i>subroutine hadvppm()</i>	<i>void hadvppm()</i>
Parameter passing	<i>hadvppm(nn, dt, dx, con, vel, area, areav, flxarr, mynn)</i>	<i>hadvppm(int *nn, float *dt, float *dx, float *con, float *vel, float *area, float *areav, float *flxarr, int *mynn)</i>
Variable precision	<i>real(kind=8) x</i>	<i>double x</i>
Built-in functions	<i>max</i>	<i>#define Max(a, b) ((a)>(b)?(a):(b))</i>
Memory read and write for multidimensional array	Column-major	Row-major
Array subscript index	Starting from any integer	Starting from 0

- 删除的内容: *nn, float*
- 删除的内容: *nn, dt*
- 删除的内容: *dx, con*
- 删除的内容: *el, area*
- 删除的内容: *av, flxarr*

444

445 **3.1.2. Converting standard C code into CUDA C**

446 After refactoring the Fortran code of the hadvppm program with standard C,

452 CUDA was used to convert the C code into CUDA C to make it computable on the
 453 GPU. A standard C program using CUDA extensions distributes a large number of
 454 copies of the kernel functions into available multiprocessors and executes them
 455 simultaneously on the GPU.

456 Figure 3 shows the GPU-HADVPPM implementation process. As mentioned in
 457 Sect. 2.1, the xyadvec program calls the hadvppm program to solve the horizontal
 458 advection function. Since the rewritten CUDA program cannot be called directly by the
 459 Fortran program (xyadvec.f), we add an intermediate subroutine (hadvppm.c) as an
 460 interface to transfer the parameters and data required for GPU computing from the
 461 xyadvec Fortran program to the hadvppm_kernel CUDA C program.

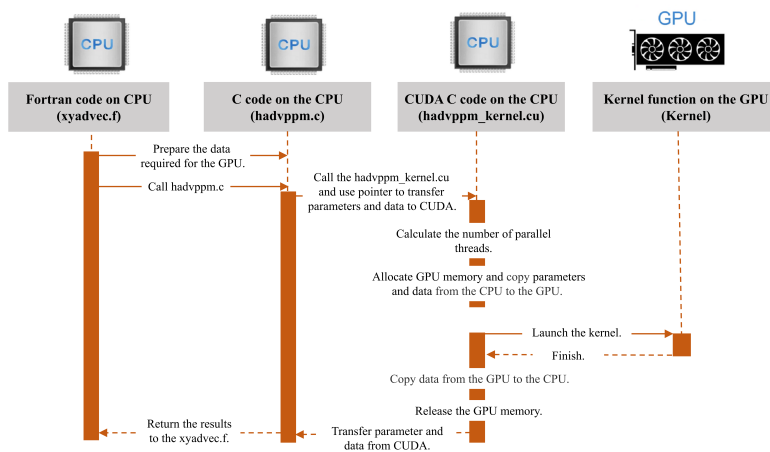
462 A CUDA program automatically uses numerous threads on the GPU to execute
 463 kernel functions. Therefore, the hadvppm_kernel CUDA C program first calculates the
 464 number of parallel threads according to the array dimension. Then, the GPU memory
 465 is allocated, and the parameters and data are copied from the CPU to the GPU. As the
 466 CUDA program launches a large number of parallel threads to execute kernel functions
 467 simultaneously, the computation results will be copied from the GPU back to the CPU.
 468 Finally, the GPU memory is released, and the data computed on the GPU are returned
 469 to the xyadvec program via the hadvppm C program.

删除的内容: the implementation process of

删除的内容: And then allocate

删除的内容: copy

删除的内容: is



470

471 **Figure 3.** The calling and computation process of the GPU-HADVPPM on the CPU-GPU

476 heterogeneous platform.

477 3.2. Coupling and optimization of the GPU-HADVPPM scheme on a single GPU

478 After the hadvppm program was rewritten with standard C and CUDA, the
479 implementation process of the HADVPPM scheme was loaded from the CPU to the
480 GPU. Then, we coupled the GPU-HADVPPM to the CAMx model. For ease of
481 description, we will refer to this original heterogeneous version of CAMx as CAMx-
482 CUDA V1.0. In CAMx-CUDA V1.0, four external loops are nested when the hadvppm
483 C program is called by the xyadvec program. This will result in widespread data
484 transfers from the CPU to the GPU over the PCIe bus within a time step, making the
485 computation of CAMx-CUDA V1.0 inefficient.

486 Therefore, we optimize the xyadvec Fortran program to significantly reduce the
487 frequency of data transmission between the CPU and GPU, increase the amount of data
488 computation on the GPU, and improve the total computing efficiency of the CAMx on
489 the CPU-GPU heterogeneous platforms. In the original CAMx-CUDA V1.0, four
490 external loops outside the hadvppm C program, and several one-dimensional arrays, are
491 computed before calling the hadvppm C program. Then, the CPU will frequently launch
492 the GPU and transfer data to it within a time step. When the code optimization is
493 completed, the three- or four-dimensional arrays required for a GPU computation
494 within a time step will be sorted before calling the hadvppm C program, and then the
495 CPU will package and transfer the arrays to the GPU in batches. An example of the
496 xyadvec Fortran program optimization is shown in Figure S1.

497 The details of the four different versions are shown in Table 3. In CAMx-CUDA
498 V1.0, the Fortran code of the HADVPPM scheme was rewritten using standard C and
499 CUDA, and the xyadvec program was not optimized. The dimensions of the c1d
500 variable array transmitted to the GPU in the X and Y directions are 157 and 145 in this
501 case, respectively. In CAMx-CUDA V1.1 and CAMx-CUDA V1.2, the c1d variable
502 transmitted from the CPU to GPU is expanded to two (approximately 23,000 numbers)
503 and four dimensions (approximately 27.4 million numbers) by optimizing the xyadvec

删除的内容: is

删除的内容: And then

删除的内容: the

删除的内容: It

删除的内容: the

删除的内容: the

删除的内容: of

删除的内容: The

删除的内容: was

删除的内容: the

删除的内容: is

删除的内容: are

删除的内容: about

删除的内容: about

518 Fortran program and hadvppm_kernel CUDA C program, respectively.

519 The order in which the data are accessed in GPU memory affects the
 520 computational efficiency of the code. In CAMx-CUDA V1.3 of Table 4, we further
 521 optimized the order in which the data are accessed in GPU memory based on the order
 522 in which they are stored in memory, and eliminated the unnecessary assignment loops
 523 that were added due to the difference in memory read order between Fortran and C.

524 As described in Sect. 2.4, a thread is the basic unit of parallelism in CUDA
 525 programming. The thread structure is organized into a three-level hierarchy. The highest
 526 level is a grid, which consists of three-dimensional thread blocks. The second level is a
 527 block, which also consists of three-dimensional threads. The built-in CUDA variable
 528 *threadIdx.x* determines a unique thread "ID" number inside a thread block. Similarly,
 529 the built-in variables *blockIdx.x* and *blockIdx.y* determine which block to execute on,
 530 and the size of the block is determined by using the built-in variable *blockDim.x*. For
 531 the two-dimensional horizontal grid points, many threads and blocks can be organized
 532 so that each CUDA thread computes the results for different spatial positions
 533 simultaneously.

534 Before CAMx-CUDA V1.4, the loops for the three-dimensional spatial grid points
 535 (i,j,k) are replaced by index computations using only the thread index ($i = threadIdx.x$
 536 $+ blockIdx.x * blockDim.x$) to use the thread indices to simultaneously compute the grid
 537 point in the x or y direction. To take full advantage of the thousands of threads in the
 538 GPU, we implement thread and block indices ($i = threadIdx.x + blockIdx.x * blockDim.x$;
 539 $j = blockIdx.y$) to simultaneously compute all the horizontal grid points (i,j) in CAMx-
 540 CUDA V1.4. This is permitted because there are no interactions among the horizontal
 541 grid points.

542 **Table 3.** The details of different CAMx-CUDA versions during optimization.

Version	Major revisions	Amount of data computation on GPU
CAMx-CUDA V1.0	The Fortran code of the HADVPPM subroutine was rewritten using standard C and CUDA, and <i>xyadvec.f</i> was not optimized.	157 and 145 in the x direction and y direction for the <i>clD</i> variable, respectively.
CAMx-CUDA V1.1	Optimize <i>xyadvec.f</i> and	157×145,

删除的内容: is

删除的内容: the

删除的内容: the

删除的内容: is

删除的内容: it is

删除的内容: ,

删除的内容: structure of

删除的内容: s

删除的内容: Built

删除的内容: Similarity,

删除的内容: variable

删除的内容: the

删除的内容: dimension

删除的内容: using

删除的内容: ,

删除的内容: indexes only computes

删除的内容: simultaneous. In order to

删除的内容: simultaneous

删除的内容: the

	<i>hadvppm_kernel.cu</i> to expand the dimension of the array transmitted to the GPU from 1-dimensional to 2-dimensional.	approximately 23,000 numbers for the c2d variable.
CAMx-CUDA V1.2	Based on the CAMx-CUDA V1.1, the dimension of the array transmitted to the GPU is extended from 2 to 4 dimensions.	157×145×14×86, approximately 27.4 million numbers for the c4d variable.
CAMx-CUDA V1.3	Based on the CAMx-CUDA V1.2, the order of GPU memory access is optimized and unnecessary assignment loops are eliminated.	157×145×14×86, approximately 27.4 million numbers for the c4d variable.
CAMx-CUDA V1.4	Based on the CAMx-CUDA V1.3, using thread and block indices ($i = threadIdx.x + blockIdx.x * blockDim.x; j = blockIdx.y$).	157×145×14×86, approximately 27.4 million numbers for the c4d variable.

删除的内容: about 2

删除的内容: about 2

删除的内容: about 2

删除的内容: about 2

562

563 3.3. MPI+CUDA acceleration algorithm of CAMx-CUDA on multiple GPUs

564 Generally, superlarge clusters have thousands of compute nodes. The current
565 CAMx V6.10, implemented by adopting MPI communication technology, typically
566 runs on dozens of compute nodes. Once the GPU-HADVPPM is coupled into the
567 CAMx, it also has to run on multiple compute nodes that are equipped with one or more
568 GPUs on each node. To make full use of multicore and multi-GPU supercomputers, and
569 further improve the overall computational performance of CAMx-CUDA, we adopt a
570 parallel architecture with an MPI+CUDA hybrid paradigm, that is, the collaborative
571 computing strategy of multiple CPU cores and multiple GPU cards is adopted during
572 the operation of the CAMx-CUDA model. Adopting this strategy, the GPU-HADVPPM
573 can run on multiple GPUs, and the Fortran code of the other modules in the CAMx-
574 CUDA model can run on multiple CPU cores.

删除的内容: super-l

删除的内容: which

删除的内容: multi-core

删除的内容: the

删除的内容: ,

删除的内容: Adopt

575 As shown in Figure 4, after the simulated region is subdivided by MPI, a CPU
576 core is responsible for the computation of a subregion. To improve the total
577 computational performance of the CAMx-CUDA model, we further used the NVIDIA
578 CUDA library to obtain the number of GPUs per node, and then used the MPI process
579 ID and remainder function to determine the GPU ID to be launched by each node.

删除的内容: is

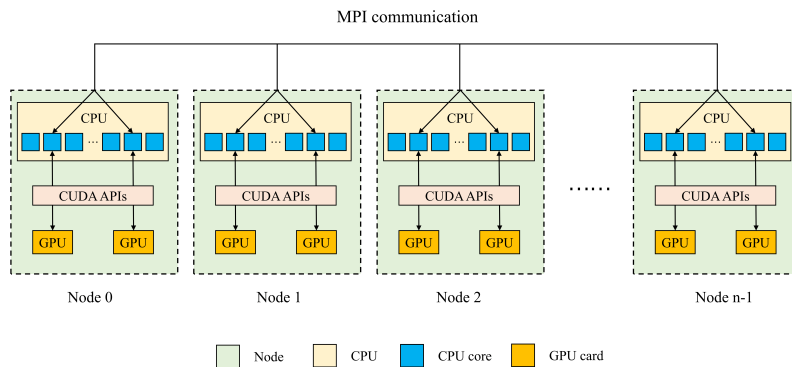
删除的内容: .

删除的内容: In order to

删除的内容: ,

594 Finally, we used the NVIDIA CUDA library, `cudaSetDevice`, to configure a GPU card
 595 for each CPU core.

596 According to the benchmark performance experiments, the parallel design of
 597 CAMx adopts the master-slave mode, and P0 is responsible for inputting and outputting
 598 data. If two processes (P0 and P1) were launched, only the P1 and its configured GPU
 599 participate in integration.



600
 601 **Figure 4.** An example of parallel architecture with an MPI+CUDA hybrid paradigm on multiple
 602 GPUs.

603 **4. Experimental results**

604 The validation and evaluation of porting the HADVPPM scheme from the CPU to
 605 the GPU platform were conducted using offline and coupling performance experiments.
 606 First, we validated the results between the different CAMx versions, and then the offline
 607 performance of the GPU-HADVPPM on a single GPU was tested by offline
 608 experiments. Finally, coupling performance experiments illustrate its potential in three
 609 dimensions with varying chemical regimes. 4.2 and 4.4, the CAMx versions of the
 610 HADVPPM scheme written in Fortran, standard C, and CUDA C, are named F, C, and
 611 CUDA C, respectively.

删除的内容: Master
 删除的内容: Slave

删除的内容: result
 删除的内容: experiment
 删除的内容: the
 删除的内容: Sect.
 删除的内容: Sect.
 删除的内容: version
 删除的内容: by
 删除的内容: language
 删除的内容: ,
 删除的内容: ,
 删除的内容: is
 删除的内容: ,

626 4.1. Experimental setup

627 The test case is a 48 h simulation covering Beijing, Tianjin and part of the Hebei
628 Province region. The horizontal resolution is 3 km with 145×157 grid boxes. The
629 model adopted 14 vertical layers. The simulation started at 12:00 UTC on 01 November
630 2020 and ended at 12:00 UTC on 03 November 2020. The meteorological fields driving
631 the CAMx model were provided by the weather research and forecasting (WRF;
632 Skamarock et al., 2008) model. The sparse matrix operator kernel emission (SMOKE;
633 Houyoux and Vukovich, 1999) version 2.4 model is used to provide gridded emission
634 data for the CAMx model. The emission inventories (Sun et al., 2022) include the
635 regional emissions in East Asia that were obtained from the transport and chemical
636 evolution over the Pacific (TRACE-P; Streets et al., 2003; Streets et al., 2006) project,
637 30-min (approximately 55.6 km at mid-latitude) spatial resolution Intercontinental
638 chemical transport experiment-Phase B (INTEX-B; Zhang et al., 2009) and the updated
639 regional emission inventories in North China. The physical and chemical numerical
640 methods selected during the CAMx model integration are listed in Table S2.

641 4.2. Error analysis

642 The hourly concentrations of different CAMx simulations (Fortran, C, and CUDA
643 C versions) are compared to verify the usefulness of the CUDA C version of CAMx for
644 numerical precision for scientific usage. Here, we chose six major species, i.e., SO₂, O₃,
645 NO₂, CO, H₂O₂ and PSO₄, after 48 h of integration to verify the results. Due to the
646 differences in programming languages and hardware, the simulation results are affected
647 during the porting process. Figures 5~7 present the spatial distributions of SO₂, O₃, NO₂,
648 CO, H₂O₂ and PSO₄, as well as the absolute errors (AEs) of their concentrations from
649 different CAMx versions. The species' spatial patterns of the three CAMx versions are
650 visually very similar. Between the Fortran and C versions, especially, the AEs in all the
651 grid boxes are in the range of ± 0.01 ppbV (the unit of PSO₄ is $\mu\text{g} \cdot \text{m}^{-3}$). During the
652 porting process, the primary error comes from converting standard C to CUDA C, and

删除的内容: 48h

删除的内容: the

删除的内容: the region of

删除的内容: province

删除的内容: 3km

删除的内容: ,

删除的内容: ,

删除的内容: ,

删除的内容: Weather

删除的内容: Research

删除的内容: Forecasting

删除的内容: Sparse

删除的内容: Matrix

删除的内容: Operator

删除的内容: Kernel

删除的内容: Emission

删除的内容: Transport

删除的内容: Chemical

删除的内容: Evolution

删除的内容: about

删除的内容: 6km

删除的内容: Chemical

删除的内容: Transport

删除的内容: Experiment

删除的内容: concentration

删除的内容: the

删除的内容: of

删除的内容: 48h

删除的内容: Figure

删除的内容: distribution

删除的内容: Especially b

684 the main reason is related to the hardware difference between the CPU and GPU. Due
685 to the slight difference in data operation and accuracy between the CPU and GPU
686 (NVIDIA,2023), the concentration variable of the hadvppm program appears to have
687 minimal negative values (approximately $-10^{-9} \sim -10^{-4}$) when integrated on the GPU.
688 To allow the program to continue running, we forcibly replace these negative values
689 with 10^{-9} . It is because these negative values are replaced by positive values that the
690 simulation results are biased. In general, for SO₂, O₃, NO₂, H₂O₂ and PSO₄, the AEs in
691 the majority of the grid boxes are in the range of ± 0.8 ppbV or $\mu\text{g} \cdot \text{m}^{-3}$ between the
692 standard C and CUDA C versions; for CO, because its background concentration is
693 higher, the AEs of the standard C and CUDA C versions are outside that range, and fall
694 into the range of -8 and 8 ppbV in some grid boxes and shows more obvious AEs than
695 the other species.

删除的内容: was

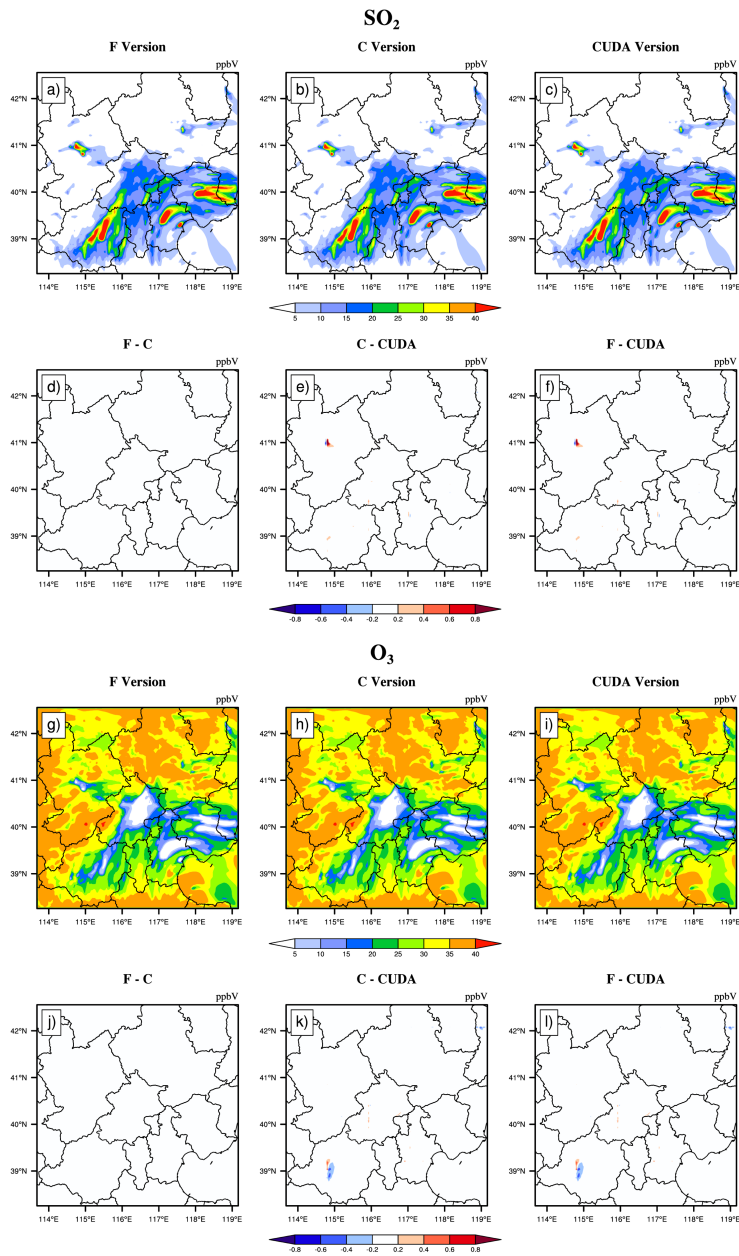
删除的内容: about

删除的内容: integrating

删除的内容: In order to

删除的内容: IfThis

删除的内容: which falls

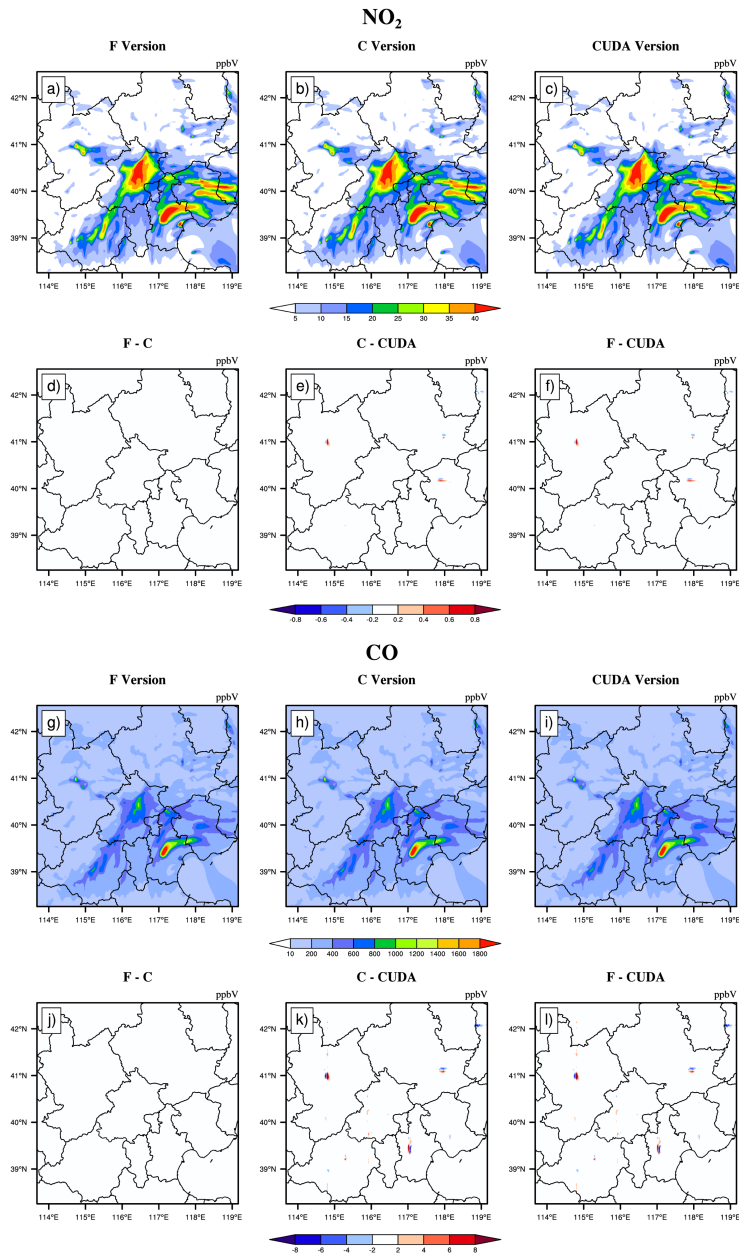


702
703

Figure 5. SO₂ and O₃ concentrations outputted by the CAMx model for the Fortran, standard C, and

704 CUDA C versions. Panels (a) and (g) are from the Fortran versions. Panels (b) and (h) are from the
705 standard C versions. Panels (c) and (i) are ~~from the~~ CUDA C versions. Panels (d) and (j) are the
706 output concentration differences of the Fortran and standard C versions. Panels (e) and (k) are the
707 output concentration differences of the standard C and CUDA C versions. Panels (f) and (l) are the
708 output concentration differences of the Fortran and CUDA C versions.

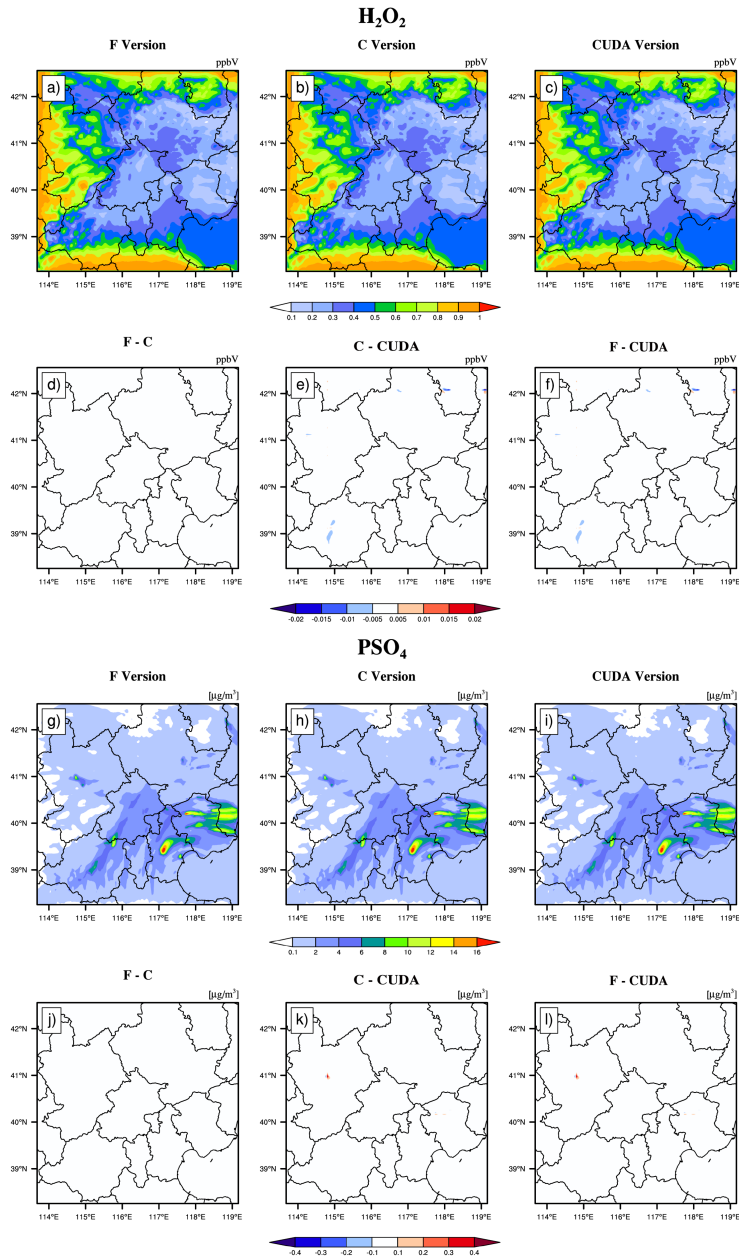
删除的内容: from



710
711

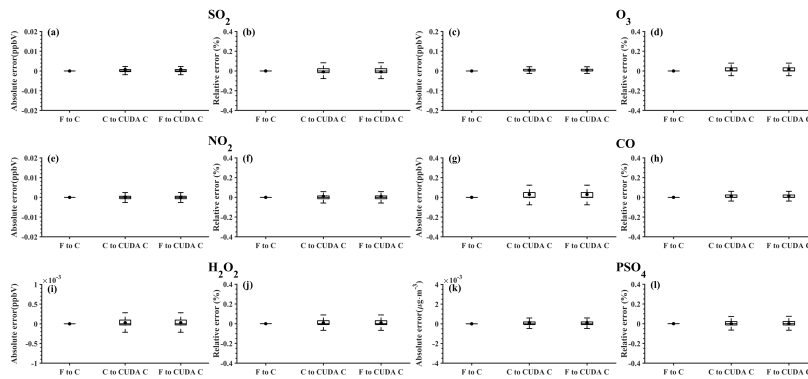
Figure 6. NO₂ and CO concentrations outputted by the CAMx model for the Fortran, standard C,

712 and CUDA C versions. Panels (a) and (g) are from the Fortran versions. Panels (b) and (h) are from
713 the standard C versions. Panels (c) and (i) are from the CUDA C versions. Panels (d) and (j) are the
714 output concentration differences of the Fortran and standard C versions. Panels (e) and (k) are the
715 output concentration differences of the standard C and CUDA C versions. Panels (f) and (l) are the
716 output concentration differences of the Fortran and CUDA C versions.



718 **Figure 7.** H₂O₂ and PSO₄ concentrations output by the CAMx model for the Fortran, standard C,
 719 and CUDA C versions. Panels (a) and (g) are from the Fortran versions. Panels (b) and (h) are from
 720 the standard C versions. Panels (c) and (i) are from the CUDA C versions. Panels (d) and (j) are the
 721 output concentration differences of Fortran and standard C versions. Panels (e) and (k) are the output
 722 concentration differences of the standard C and CUDA C versions. Panels (f) and (l) are the output
 723 concentration differences of the Fortran and CUDA C versions.

724 Figure 8 shows the boxplot of the AEs and relative error (REs) in all the grid boxes
 725 for the six species during the porting process. As described above, the AEs and REs
 726 introduced by Fortran to the standard C code refactoring process are significantly small,
 727 and the primary error comes from converting standard C to CUDA C. Statistically, the
 728 average AEs (REs) of SO₂, O₃, NO₂, CO, H₂O₂ and PSO₄ were -0.0009 ppbV (-0.01%),
 729 0.0004 ppbV (-0.004%), 0.0005 ppbV (0.008%), 0.03 ppbV (0.01%), 2.1×10^{-5}
 730 ppbV (-0.01%) and $0.0002 \mu\text{g} \cdot \text{m}^{-3}$ (0.0023%), respectively, between the Fortran
 731 and CUDA C versions. In terms of the time series, the regionally averaged time series
 732 of the three versions are almost consistent (as shown in Figure S2), and the maximum
 733 AEs for the above six species are 0.001 ppbV, 0.005 ppbV, 0.002 ppbV, 0.03 ppbV,
 734 0.0001 ppbV and $0.0002 \mu\text{g} \cdot \text{m}^{-3}$, respectively, between the Fortran and CUDA C
 735 versions.



736 **Figure 8.** The distributions of absolute errors and relative errors for SO₂, O₃, NO₂, CO, H₂O₂ and
 737 PSO₄ in all of the grid boxes after 48 hours of integration.
 738

739 Figure 9 presents the regionally averaged time series and the AEs of SO₂, O₃, NO₂,

删除的内容: outputted

删除的内容: .

删除的内容: the

删除的内容: of

删除的内容: is

删除的内容: 001ppbV

删除的内容: ppbV

删除的内容: ppbV

删除的内容: 03ppbV

删除的内容: ppbV

删除的内容: .

751 CO, H₂O₂ and PSO₄. The time series between the different versions is almost consistent,
752 and the maximum AEs for the above six species are 0.001 ppbv, 0.005 ppbv, 0.002
753 ppbv, 0.03 ppbv, 0.0001 ppbv and 0.0002 $\mu\text{g} \cdot \text{m}^{-3}$, respectively, between the Fortran
754 and CUDA C versions.

755 It is difficult to verify the scientific applicability of the results from the CUDA C
756 version because the programming language and hardware are different between the
757 Fortran and CUDA C versions. Here, we used the evaluation method of Wang et al.
758 (2021a) to compute the root mean square errors (RMSEs) of SO₂, O₃, NO₂, CO, H₂O₂
759 and PSO₄ between the Fortran and CUDA C versions, which are 0.0007 ppbV, 0.001
760 ppbV, 0.0002 ppbV, 0.0005 ppbV, 0.00003 ppbV and 0.0004 $\mu\text{g} \cdot \text{m}^{-3}$, respectively,
761 much smaller than the spatial variation of the whole region, which is 7.0 ppbV
762 (approximately 0.004%), 9.7 ppbV (approximately 0.003%), 7.4 ppbV (approximately
763 0.003%), 142.2 ppbV (approximately 0.006%), 0.2 ppbv (approximately 0.015%) and
764 1.7 $\mu\text{g} \cdot \text{m}^{-3}$ (approximately 0.004%). The bias between CUDA C and the Fortran
765 version of the above six species is negligible compared with their own spatial changes,
766 and the results of the CUDA C version are generally acceptable for research purposes.
767

768 4.3. Offline performance comparison of GPU-HADVPPM

769 As described in Sect. 4.2, we validate that the CAMx model result of the CUDA
770 C version is generally acceptable for scientific research. We tested the offline
771 performance of the HADVPPM and GPU-HADVPPM schemes on 1 CPU core and 1
772 GPU card. There are 7 variables input into the HADVPPM program, which are nn, dt,
773 dx, con, vel, area and areav, and their specific meanings are shown in Table S1.

774 First, we use the random number function in Fortran to create random single-
775 precision floating-point numbers of different sizes for the above 7 variables, and then
776 transmit these random numbers to the hadvppm Fortran program and hadvppm_kernel
777 CUDA C program for computation. Finally, we test the offline performance of the
778 HADVPPM and GPU-HADVPPM on the CPU and GPU platforms. During the offline
779 performance experiments, we used two different CPUs and GPUs described in Sect.

删除的内容: 001ppbV

删除的内容: ppbV

删除的内容: ppbV

删除的内容: 03ppbV

删除的内容: ppbV

删除的内容:

删除的内容: version

删除的内容: ,

删除的内容: 2ppbV

删除的内容: It is indicated that the

删除的内容: the

删除的内容: can b

删除的内容: e

删除的内容: scheme

删除的内容: , respectively

删除的内容: ,

删除的内容: Firstly

删除的内容: ,

删除的内容: , respectively

删除的内容: the

800 2.4., and the experimental results are shown in Figure 9.

801 On the CPU platform, the wall time of the hadvppm Fortran program does not
802 change significantly when the data size is less than 1000. With the increase in the data
803 size, its wall time increases linearly. When the data size reaches 10^7 , the wall time of
804 the hadvppm Fortran program on the Intel Xeon E5-2682v4 and Intel Platinum 8168
805 CPU platforms is 1737.3 ms and 1319.0 ms, respectively. On the GPU platform, the
806 reconstructed and extended CUDA C program implements parallel computation of
807 multiple grid points by executing a large number of kernel function copies, so the
808 computational efficiency of the hadvppm_kernel CUDA C code on it is significantly
809 improved. In the size of 10^7 random numbers, the hadvppm_kernel CUDA C program
810 takes only 12.1 ms and 1.6 ms to complete the computation on the NVIDIA Tesla K40m
811 and NVIDIA Tesla V100 GPU.

812 Figure 9. (b) shows the speedup of HADVPPM and GPU-HADVPPM on the CPU
813 platform and GPU platform under different data sizes. When mapping the HADVPPM
814 scheme to the GPU, the computational efficiency under different data sizes is not only
815 significantly improved, but the larger the data size is, the more obvious the acceleration
816 effect of the GPU-HADVPPM. For example, in the size of 10^7 random numbers, the
817 GPU-HADVPPM achieved a 1113.6x and 845.4x acceleration on the NVIDIA Tesla
818 V100 GPU, respectively, compared to the two CPU platforms. Although the K40m
819 GPU's single-card computing performance is slightly lower than that of the V100 GPU,
820 GPU-HADVPPM can also achieve up to a 143.3x and 108.8x acceleration.

821 As described in Sect. 3.2, the thread is the most basic GPU unit for parallel
822 computing. Each dimension of the three-dimensional block can contain a maximum
823 number of threads of 1024, 1024 and 64. Each dimension of the three-dimensional grid
824 can contain a maximum number of blocks of $2^{31} - 1$, 65535, and 65535. It is
825 theoretically possible to distribute a large number of copies of kernel functions into tens
826 of billions of threads for parallel computing without exceeding the GPU memory. In
827 the offline performance experiments, the GPU achieved up to 10 million threads of
828 parallel computing, while the CPU can only use serial cyclic computation. Therefore,

删除的内容: 3ms

删除的内容: 0ms

删除的内容: 1ms

删除的内容: 6ms

删除的内容: size

删除的内容: also

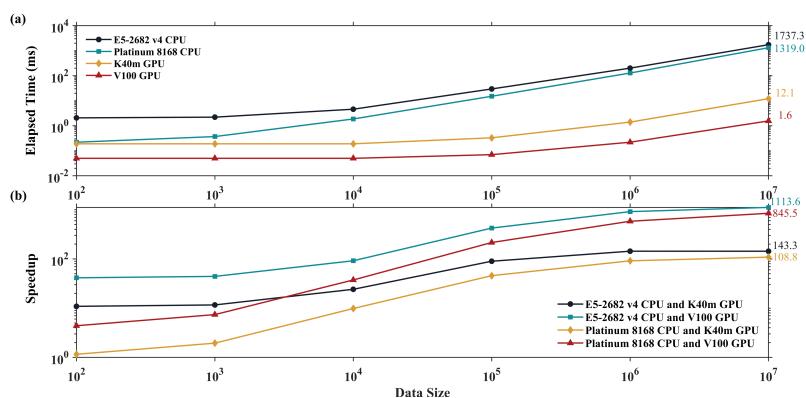
删除的内容: unit of

删除的内容: ,

删除的内容: , respectively

838 GPU-HADVPPM achieves a maximum acceleration of approximately 1100x without
 839 I/O. In addition to this study, the GPU-based SBU-YLIN scheme in the WRF model
 840 can achieve a 896x acceleration compared to the Fortran implementation running on
 841 the CPU (Mielikainen et al., 2012b).

删除的内容: about



842
 843 **Figure 9.** The offline performance of the HADVPPM and GPU-HADVPPM scheme on the CPU
 844 and GPU. The unit of the wall times for the offline performance experiments is milliseconds (ms).

删除的内容: millisecond

845 4.4. Coupling performance comparison of GPU-HADVPPM with different GPU 846 configurations

847 4.4.1. CAMx-CUDA on a single GPU

848 The offline performance results show that the larger the data size is, the more
 849 obvious the acceleration effect of the GPU-HADVPPM scheme. After coupling the
 850 GPU-HADVPPM to CAMx without changing the advection module algorithm, the
 851 overall computational efficiency of the CAMx-CUDA model is extremely low, and it
 852 takes approximately 621 minutes to complete a one-hour integration on the V100
 853 cluster. Therefore, according to the optimization scheme in Sect. 3.2, by optimizing the
 854 algorithm of the xyadvec Fortran program, we gradually increase the size of the data
 855 transmitted and reduce the data transmission frequency between the CPU and GPU.
 856 When the data transmission frequency between the CPU and GPU is reduced to 1 within
 857 one time step, we further optimize the GPU memory access order on the GPU card,

删除的内容: Offline

删除的内容: about

删除的内容: frequency of

删除的内容: -

864 eliminate unnecessary assignment loops before kernel functions are launched and use
865 the thread and block indices.

866 Table 4 lists the total elapsed time for different versions of the CAMx-CUDA
867 model during the optimization, as described in Section 3.2. Since the xyadvec program
868 in CAMx-CUDA V1.0 is not optimized, it is extremely computationally inefficient
869 when starting two CPU processes and configuring a GPU card for P1. On the K40m
870 and V100 clusters, it takes 10829 seconds and 37237 seconds, respectively, to complete
871 a 1-hour simulation.

872 By optimizing the algorithm of the xyadvec Fortran program and hadvppm_kernel
873 CUDA C program, the data transmission frequency between the CPU and GPU was
874 decreased, and the overall computing efficiency was improved after GPU-HADVPPM
875 was coupled to the CAMx-CUDA model. In CAMx-CUDA V1.2, the data transmission
876 frequency between CPU-GPU within one time step is reduced to 1, the elapsed time on
877 the two heterogeneous clusters is 1207 seconds and 548 seconds, respectively, and the
878 speedup is 9.0x and 68.0x compared to CAMx-CUDA V1.0.

879 The GPU memory access order can directly affect the overall GPU-HAVPPM
880 computational efficiency on the GPU. In CAMx-CUDA V1.3, we optimized the
881 memory access order of the hadvppm_kernel CUDA C program on the GPU and
882 eliminated the unnecessary assignment loops before the kernel functions were launched,
883 which further improved the CAMx-CUDA model's computational efficiency, resulting
884 in 12.7x and 94.8x speedups.

885 Using thread and block indices to simultaneously compute the horizontal grid
886 points can greatly improve the computational efficiency of the GPU-HADVPPM and
887 thus reduce the overall elapsed time of the CAMx-CUDA model. CAMx-CUDA V1.4
888 further reduces the elapsed time by 378 seconds and 103 seconds on the K40m cluster
889 and V100 cluster, respectively, compared with CAMx-CUDA V1.3, and achieves up to
890 a 29.0x and 128.4x speedup compared with CAMx-CUDA V1.0.

891 **Table 4.** Total elapsed time for different versions of CAMx-CUDA during the optimization. The
892 unit of elapsed time for experiments is in seconds (s).

删除的内容: .

删除的内容: the

删除的内容: cluster

删除的内容: frequency of

删除的内容: coupling

删除的内容: frequency of

删除的内容: and

删除的内容: the

删除的内容: of GPU-HAVPPM

删除的内容: have

删除的内容: simultaneous

删除的内容: respectively on

删除的内容: ,

删除的内容: achieving

Versions	K40m cluster		V100 cluster	
	Elapsed Time	Speedup	Elapsed Time	Speedup
CAMx-CUDA V1.0	10829	1.0	37237	1.0
CAMx-CUDA V1.1	1403	7.7	1082	34.4
CAMx-CUDA V1.2	1207	9.0	548	68.0
CAMx-CUDA V1.3	751	12.7	393	94.8
CAMx-CUDA V1.4	373	29.0	290	128.4

带格式的: 右

带格式的: 右

带格式的: 右

带格式的: 右

带格式的: 右

907 In terms of the single module computational efficiency of HADVPPM and GPU-
908 HADVPPM, we further tested the computational performance of the Fortran version of
909 HADVPPM on the CPU, C version of HADVPPM on the CPU, and the CUDA C
910 version of GPU-HADVPPM in CAMx-CUDA V1.4 (GPU-HADVPPM V1.4) on the
911 GPU, using system clock functions in the Fortran language and cudaEvent_t in CUDA
912 programming. The specific results are shown in Figure 10. On the K40m cluster, it takes
913 37.7 seconds and 51.4 seconds to launch the Intel Xeon E5-2682 v4 CPU to run the
914 Fortran and C version HADVPPM, respectively, and the C version is 26.7% slower
915 than the Fortran version. After the CUDA technology was used to convert the C code
916 into CUDA C, the CUDA C version took 29.6 seconds to launch an NVIDIA Tesla
917 K40m GPU to run GPU-HADVPPM V1.4, with a 1.3x and 1.7x acceleration. On the
918 V100 cluster, the Fortran, C, and CUDA C versions are computationally more efficient
919 than those on the K40m cluster. It takes 30.1 seconds and 45.2 seconds to launch the
920 Intel Xeon Platinum 8168 CPU to run the Fortran and C version HADVPPM, and 1.6
921 seconds to run the GPU-HADVPPM V1.4 using an NVIDIA V100 GPU. The
922 computational efficiency of the CUDA C version is 18.8x and 28.3x higher than the
923 Fortran and C versions, respectively.

删除的内容: coupling test

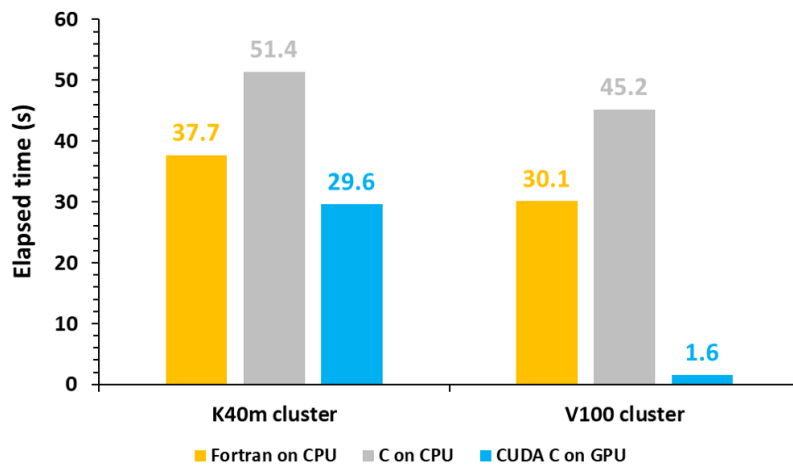
删除的内容: ,

删除的内容: ,

删除的内容: the

删除的内容: the

删除的内容: version



930

931 **Figure 10.** The elapsed time of the Fortran version HADVPPM on the CPU, the C version
 932 HADVPPM on the CPU, and the CUDA C version GPU-HADVPPM V1.4 on the GPU. The unit is
 933 in seconds (s).

删除的内容: ,

934 **4.4.2. CAMx-CUDA on multiple GPUs**

935 To make full use of the multicore and multi-GPUs in the heterogeneous cluster,
 936 the MPI+CUDA acceleration algorithm was implemented to improve the total
 937 computational performance of the CAMx-CUDA model. Two different compile flags
 938 were implemented in this study before comparing the computational efficiency of
 939 CAMx-CUDA V1.3 and V1.4 on multiple GPUs, namely, *-mieee-fp* and *-fp-model*
 940 *precise*. The *-mieee-fp* compile flag comes from the *Makefile* of the official CAMx
 941 version, which uses the IEEE standard to compare the floating-point numbers. Its
 942 computational accuracy is higher, but the efficiency is slower. The *-fp-model precise*
 943 compile flag controls the balance between the precision and efficiency of the floating-
 944 point calculations, and it can force the compiler to use the vectorization of some
 945 calculations under value safety. The experimental results show that the *-fp model*
 946 *precise* compile flag is 41.4% faster than *-mieee-fp*, and the AEs of the simulation
 947 results are less than ± 0.05 ppbv (Figure S3). Therefore, the *-fp model precise* compile
 948 flag is implemented when comparing the computational efficiency of CAMx-CUDA

删除的内容: multi-core

删除的内容: ,

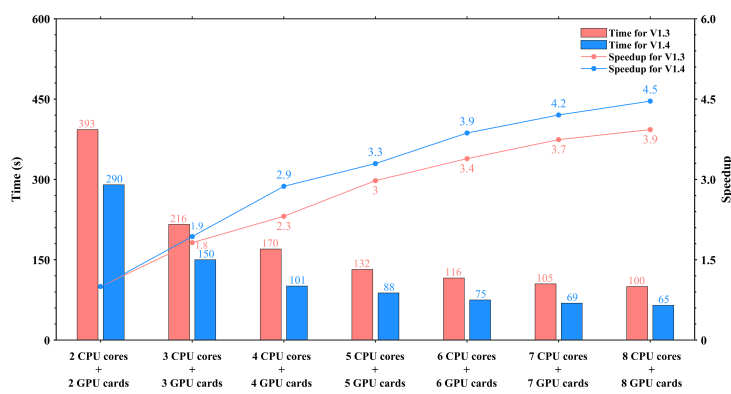
删除的内容: control

删除的内容: the value-safe. The experiment

删除的内容: 05ppbV

955 V1.3 and V1.4 on multiple GPU cards. Figure 11 shows the total elapsed time and
 956 speedup of CAMx-CUDA V1.3 and V1.4 on the V100 cluster. The total elapsed time
 957 decreases as the number of CPU cores and GPU cards increases. When starting 8 CPU
 958 cores and 8 GPU cards, the speedup of CAMx-CUDA V1.4 is increased from 3.9x to
 959 4.5x compared with V1.3, and the computational efficiency is increased by 35.0%.

删除的内容: .



960

961 **Figure 11.** The total elapsed time and speedup of CAMx-CUDA V1.3 and V1.4 on multiple
 962 GPUs. The unit of elapsed time for experiments is in seconds (s).

删除的内容:

963 **5. Conclusions and discussion**

964 GPU accelerators are playing an increasingly important role in high-performance
 965 computing. In this study, a GPU acceleration version of the PPM solver (GPU-
 966 HADVPPM) of horizontal advection for an air quality model was developed, which
 967 runs on GPU accelerators using the standard C programming language and CUDA
 968 technology. The offline performance experimental results showed that the K40m and
 969 V100 GPU can achieve up to a 845.4x and 1113.6x speedup, respectively, and the larger
 970 the data input to the GPU, the more obvious the acceleration effect. After coupling the
 971 GPU-HADVPPM to the CAMx model, a series of optimization measures were taken,
 972 including reducing the CPU-GPU communication frequency, increasing the data

删除的内容: is

删除的内容: that

删除的内容: can be

删除的内容: Offline

删除的内容: experiments

删除的内容: are

删除的内容: size of

982 computation_size on the GPU, optimizing the GPU memory access order, and using
 983 thread and block indices to improve the overall computing performance of the CAMx-
 984 CUDA model. Using a single GPU card, the optimized CAMx-CUDA V1.4 model
 985 improved the computing efficiency by 29.0x and 128.4x on the K40m cluster and the
 986 V100 cluster, respectively. In terms of the single-module computational efficiency of
 987 GPU-HADVPPM, it achieved a 1.3x and 18.8x speedup on an NVIDIA Tesla K40m
 988 GPU and NVIDIA Tesla V100 GPU, respectively. To make full use of the multicore and
 989 multi-GPU supercomputers and further improve the total computational performance
 990 of the CAMx-CUDA model, a parallel architecture with an MPI+CUDA hybrid
 991 paradigm was presented. After implementing the acceleration algorithm, the total
 992 elapsed time decreased as the number of CPU cores and GPU cards increased, and it
 993 achieved up to a 4.5x speedup when launching 8 CPU cores and 8 GPU cards compared
 994 with 2 CPU cores and 2 GPU cards.

995 However, the current approach has some limitations, which are as follows:

996 1) We currently implement thread and block coindexing to compute horizontal
 997 grid points in parallel. Given the CAMx Model 3-dimensional grid computing
 998 characteristics, in the future, 3-dimensional thread and block coindexing will be
 999 considered to compute 3-dimensional grid points in parallel.

1000 2) The communication bandwidth of data transfer is one of the main issues
 1001 restricting the computing performance of the CUDA C codes on the GPUs. This
 1002 restriction holds true not only for GPU-HADVPPM, but also for the WRF module,
 1003 (Mielikainen et al., 2012b; Mielikainen et al., 2013b; Huang et al., 2013). In this study,
 1004 the data transmission efficiency between the CPU and GPU is improved only by
 1005 reducing the communication frequency. In the future, more technologies, such as
 1006 pinned memory (Wang et al., 2016), will be considered to resolve the communication
 1007 bottleneck between the CPUs and GPUs.

1008 3) To further improve the overall computational efficiency of the CAMx model,
 1009 the heterogeneous porting scheme proposed in this study will be considered to conduct
 1010 the heterogeneous porting of other CAMx modules in the future.

删除的内容: ,

删除的内容: improves

删除的内容: can

删除的内容: multi-core

删除的内容: is

删除的内容: decreases

删除的内容: increases

删除的内容: can

删除的内容: launch

删除的内容: there are some limitations of

删除的内容: implemented

删除的内容: co-indexing

删除的内容: model

删除的内容: co-indexing

删除的内容: for

删除的内容: holds true

删除的内容: ,

删除的内容: as well

删除的内容: CPU

删除的内容: GPU

删除的内容: In order to

删除的内容: carry out

1033

1034 *Code and data availability.* The source codes of CAMx version 6.10 are available at
1035 <https://camx-wp.azurewebsites.net/download/source/> (last access: 24 March 2023,
1036 ENVIRON,2022). The dataset related to this paper and the CAMx-CUDA codes are
1037 available online via ZENODO (<http://doi.org/10.5281/zenodo.7765218>; Cao et
1038 al.,2023).

删除的内容: the

删除的内容: e/

1039

1040 *Author contributions.* KC conducted the simulation and prepared the materials. QZW,
1041 LLW, and LNW planned and organized the project. KC, QZW and XT refactored and
1042 optimized the codes. LLW, NW, HQC, and DQL collected and prepared the data for
1043 simulation. KC, QZW, XT, and LNW participated in the discussion.

删除的内容: ,

删除的内容: ,

删除的内容: ,

删除的内容: took part

1044

1045 *Competing interests.* The authors declare that they have no conflicts of interest.

删除的内容: conflict

1046

1047 **Acknowledgements.** The National Key R&D Program of China (2020YFA0607804 &
1048 2017YFC0209805), the National Supercomputing Center in Zhengzhou Innovation
1049 Ecosystem Construction Technology Special Program (Grant No. 201400210700), and
1050 the Beijing Advanced Innovation Program for Land Surface funded this work. The
1051 research is supported by the High Performance Scientific Computing Center (HSCC)
1052 of Beijing Normal University and the National Supercomputing Center in Zhengzhou.

删除的内容:

删除的内容: and

删除的内容: ,

删除的内容: support

1053

1054 **References**

删除的内容: Reference

1055 Bleichrodt, F., Bisseling, R. H., and Dijkstra, H. A.: Accelerating a barotropic ocean
1056 model using a GPU, *Ocean Modelling*, 41, 16-21, 10.1016/j.ocemod.2011.10.001,
1057 2012.

1058 Cao, K., Wu, Q., Wang, L., Wang, N., Cheng, H., Tang, X., Li, D., and Wang, L.: The
1059 dataset of the manuscript "GPU-HADVPPM V1.0: high-efficient parallel GPU

1072 design of the Piecewise Parabolic Method (PPM) for horizontal advection in air
1073 quality model (CAMx V6.10)", ZENODO,
1074 <https://doi.org/10.5281/zenodo.7765218>, 2023.

1075 Colella, P. and Woodward, P. R.: The Piecewise Parabolic Method (PPM) for gas-
1076 dynamical simulations, *Journal of Computational Physics*, 54, 174-201,
1077 [https://doi.org/10.1016/0021-9991\(84\)90143-8](https://doi.org/10.1016/0021-9991(84)90143-8), 1984.

1078 ENVIRON: User Guide for Comprehensive Air Quality Model with Extensions
1079 Version 6.1, available at: [https://camx-wp.azurewebsites.net/Files/CAMxUsers](https://camx-wp.azurewebsites.net/Files/CAMxUsersGuide_v6.10.pdf)
1080 [Guide v6.10.pdf](https://camx-wp.azurewebsites.net/Files/CAMxUsersGuide_v6.10.pdf) (last access: 19 December 2022), 2014

1081 Govett, M., Rosinski, J., Middlecoff, J., Henderson, T., Lee, J., MacDonald, A., Wang,
1082 N., Madden, P., Schramm, J., and Duarte, A.: Parallelization and Performance of
1083 the NIM Weather Model on CPU, GPU, and MIC Processors, *Bulletin of the*
1084 *American Meteorological Society*, 98, 2201-2213, 10.1175/bams-d-15-00278.1,
1085 2017.

1086 Houyoux, M. R. and Vukovich, J. M.: Updates to the Sparse Matrix Operator Kernel
1087 Emissions (SMOKE) Modeling System and Integration with Models-3,
1088 Huang, B., Mielikainen, J., Plaza, A. J., Huang, B., Huang, A. H. L., and Goldberg, M.
1089 D.: GPU acceleration of WRF WSM5 microphysics, *High-Performance*
1090 *Computing in Remote Sensing*, 10.1117/12.901826, 2011.

1091 Huang, B., Huang, M., Mielikainen, J., Huang, B., Huang, H. L. A., Goldberg, M. D.,
1092 and Plaza, A. J.: On the acceleration of Eta Ferrier Cloud Microphysics Scheme in
1093 the Weather Research and Forecasting (WRF) model using a GPU, *High-*
1094 *Performance Computing in Remote Sensing II*, 10.1117/12.976908, 2012.

1095 Huang, M., Huang, B., Chang, Y.-L., Mielikainen, J., Huang, H.-L. A., and Goldberg,
1096 M. D.: Efficient Parallel GPU Design on WRF Five-Layer Thermal Diffusion
1097 Scheme, *IEEE Journal of Selected Topics in Applied Earth Observations and*
1098 *Remote Sensing*, 8, 2249-2259, 10.1109/jstars.2015.2422268, 2015.

1099 Huang, M., Huang, B., Mielikainen, J., Huang, H. L. A., Goldberg, M. D., and Mehta,
1100 A.: Further Improvement on GPU-Based Parallel Implementation of WRF 5-Layer

1101 Thermal Diffusion Scheme, 2013 International Conference on Parallel and
1102 Distributed Systems, 10.1109/icpads.2013.126, 2013.

1103 Jiang, J., Lin, P., Wang, J., Liu, H., Chi, X., Hao, H., Wang, Y., Wang, W., and Zhang,
1104 L.: Porting LASG/ IAP Climate System Ocean Model to Gpus Using OpenAcc,
1105 IEEE Access, 7, 154490-154501, 10.1109/access.2019.2932443, 2019.

1106 Mielikainen, J., Huang, B., Huang, H.-L. A., and Goldberg, M. D.: GPU Acceleration
1107 of the Updated Goddard Shortwave Radiation Scheme in the Weather Research
1108 and Forecasting (WRF) Model, IEEE Journal of Selected Topics in Applied Earth
1109 Observations and Remote Sensing, 5, 555-562, 10.1109/jstars.2012.2186119,
1110 2012a.

1111 Mielikainen, J., Huang, B., Huang, H.-L. A., and Goldberg, M. D.: GPU
1112 Implementation of Stony Brook University 5-Class Cloud Microphysics Scheme
1113 in the WRF, IEEE Journal of Selected Topics in Applied Earth Observations and
1114 Remote Sensing, 5, 625-633, 10.1109/jstars.2011.2175707, 2012b.

1115 Mielikainen, J., Huang, B., Huang, H. L. A., Goldberg, M. D., and Mehta, A.: Speeding
1116 Up the Computation of WRF Double-Moment 6-Class Microphysics Scheme with
1117 GPU, Journal of Atmospheric and Oceanic Technology, 30, 2896-2906,
1118 10.1175/jtech-d-12-00218.1, 2013a.

1119 Mielikainen, J., Huang, B., Wang, J., Allen Huang, H. L., and Goldberg, M. D.:
1120 Compute unified device architecture (CUDA)-based parallelization of WRF
1121 Kessler cloud microphysics scheme, Computers & Geosciences, 52, 292-299,
1122 10.1016/j.cageo.2012.10.006, 2013b.

1123 NVIDIA: CUDA C++ Programming Guide Version 10.2, available at:
1124 [https://docs.nvidia.com/cuda/archive/10.2/pdf/CUDA_C_Programming_Guide.p](https://docs.nvidia.com/cuda/archive/10.2/pdf/CUDA_C_Programming_Guide.pdf)
1125 [df](https://docs.nvidia.com/cuda/archive/10.2/pdf/CUDA_C_Programming_Guide.pdf) (last access: 19 December 2022), 2020

1126 NVIDIA: Floating Point and IEEE 754 Compliance for NVIDIA GPUs. Release 12.1,
1127 available at: <https://docs.nvidia.com/cuda/floating-point/#differences-from-x86>
1128 (last access: 18 May 2023), 2023.

1129 Odman, M. and Ingram, C.: Multiscale Air Quality Simulation Platform (MAQSIP):

1130 Source Code Documentation and Validation, 1996.

1131 Price, E., Mielikainen, J., Huang, M., Huang, B., Huang, H.-L. A., and Lee, T.: GPU-
1132 Accelerated Longwave Radiation Scheme of the Rapid Radiative Transfer Model
1133 for General Circulation Models (RRTMG), IEEE Journal of Selected Topics in
1134 Applied Earth Observations and Remote Sensing, 7, 3660-3667,
1135 10.1109/jstars.2014.2315771, 2014.

1136 Skamarock, W. C., Klemp, J. B., Dudhia, J., Gill, D. O., Barker, D.M., Duda, M. G.,
1137 Huang, X. Y., Wang, W., and Powers, J. G.: A Description of the Advanced
1138 Research WRF Version3 (No.NCAR/TN-475CSTR), University Corporation for
1139 Atmospheric Research, <https://doi.org/10.5065/D68S4MVH>, NCAR, 2008.

1140 Streets, D. G., Zhang, Q., Wang, L., He, K., Hao, J., Wu, Y., Tang, Y., and Carmichael,
1141 G. R.: Revisiting China's CO emissions after the Transport and Chemical
1142 Evolution over the Pacific (TRACE-P) mission: Synthesis of inventories,
1143 atmospheric modeling, and observations, Journal of Geophysical Research:
1144 Atmospheres, 111, <https://doi.org/10.1029/2006JD007118>, 2006.

1145 Streets, D. G., Bond, T. C., Carmichael, G. R., Fernandes, S. D., Fu, Q., He, D., Klimont,
1146 Z., Nelson, S. M., Tsai, N. Y., Wang, M. Q., Woo, J. H., and Yarber, K. F.: An
1147 inventory of gaseous and primary aerosol emissions in Asia in the year 2000,
1148 Journal of Geophysical Research: Atmospheres, 108,
1149 <https://doi.org/10.1029/2002JD003093>, 2003.

1150 Sun, Y., Wu, Q., Wang, L., Zhang, B., Yan, P., Wang, L., Cheng, H., Lv, M., Wang, N.,
1151 and Ma, S.: Weather Reduced the Annual Heavy Pollution Days after 2016 in
1152 Beijing, Sola, 18, 135-139, 10.2151/sola.2022-022, 2022.

1153 Wahib, M. and Maruyama, N.: Highly optimized full GPU-acceleration of non-
1154 hydrostatic weather model SCALE-LES, 2013 IEEE International Conference on
1155 Cluster Computing (CLUSTER), 23-27 Sept. 2013, 1-8,
1156 10.1109/CLUSTER.2013.6702667,

1157 Wang, P., Jiang, J., Lin, P., Ding, M., Wei, J., Zhang, F., Zhao, L., Li, Y., Yu, Z., Zheng,
1158 W., Yu, Y., Chi, X., and Liu, H.: The GPU version of LASG/IAP Climate System

1159 Ocean Model version 3 (LICOM3) under the heterogeneous-compute interface for
1160 portability (HIP) framework and its large-scale application, *Geosci. Model Dev.*,
1161 14, 2781-2799, 10.5194/gmd-14-2781-2021, 2021a.

1162 Wang, Y., Guo, M., Zhao, Y., and Jiang, J.: GPUs-RRTMG_LW: high-efficient and
1163 scalable computing for a longwave radiative transfer model on multiple GPUs,
1164 *The Journal of Supercomputing*, 77, 4698-4717, 10.1007/s11227-020-03451-3,
1165 2021b.

1166 Wang, Z., Wang, Y., Wang, X., Li, F., Zhou, C., Hu, H., and Jiang, J.: GPU-
1167 RRTMG_SW: Accelerating a Shortwave Radiative Transfer Scheme on GPU,
1168 *IEEE Access*, 9, 84231-84240, 10.1109/access.2021.3087507, 2016.

1169 Xiao, H., Lu, Y., Huang, J., and Xue, W.: An MPI+OpenACC-based PRM scalar
1170 advection scheme in the GRAPES model over a cluster with multiple CPUs and
1171 GPUs, *Tsinghua Science and Technology*, 27, 164-173,
1172 10.26599/TST.2020.9010026, 2022.

1173 Xu, S., Huang, X., Oey, L. Y., Xu, F., Fu, H., Zhang, Y., and Yang, G.: POM.gpu-v1.0:
1174 a GPU-based Princeton Ocean Model, *Geoscientific Model Development*, 8,
1175 2815-2827, 10.5194/gmd-8-2815-2015, 2015.

1176 Zhang, Q., Streets, D. G., Carmichael, G. R., He, K. B., Huo, H., Kannari, A., Klimont,
1177 Z., Park, I. S., Reddy, S., Fu, J. S., Chen, D., Duan, L., Lei, Y., Wang, L. T., and
1178 Yao, Z. L.: Asian emissions in 2006 for the NASA INTEX-B mission, *Atmos.*
1179 *Chem. Phys.*, 9, 5131-5153, 10.5194/acp-9-5131-2009, 2009.

第 3 页: [1] 删除的内容

Editor



第 3 页: [1] 删除的内容

Editor



第 3 页: [1] 删除的内容

Editor



第 3 页: [1] 删除的内容

Editor



第 3 页: [1] 删除的内容

Editor



第 3 页: [1] 删除的内容

Editor



第 3 页: [1] 删除的内容

Editor



第 3 页: [1] 删除的内容

Editor



第 3 页: [1] 删除的内容

Editor

▼
▲
第 3 页: [1] 删除的内容

Editor

▼
▲
第 3 页: [1] 删除的内容

Editor

▼
▲
第 3 页: [1] 删除的内容

Editor

▼
▲
第 3 页: [1] 删除的内容

Editor

▼
▲
第 3 页: [1] 删除的内容

Editor

▼
▲
第 3 页: [1] 删除的内容

Editor

▼
▲
第 3 页: [1] 删除的内容

Editor

▼
▲
第 3 页: [1] 删除的内容

Editor

第 3 页: [1] 删除的内容 Editor

第 3 页: [1] 删除的内容 Editor

第 3 页: [1] 删除的内容 Editor

第 3 页: [1] 删除的内容 Editor

第 3 页: [1] 删除的内容 Editor

第 3 页: [1] 删除的内容 Editor

第 3 页: [1] 删除的内容 Editor

第 3 页: [1] 删除的内容 Editor

第 3 页: [2] 删除的内容

Editor



第 3 页: [2] 删除的内容

Editor



第 3 页: [2] 删除的内容

Editor



第 3 页: [2] 删除的内容

Editor



第 3 页: [2] 删除的内容

Editor



第 3 页: [2] 删除的内容

Editor



第 3 页: [2] 删除的内容

Editor



第 3 页: [2] 删除的内容

Editor



第 3 页: [2] 删除的内容

Editor

▼ ←
▲
第 3 页: [2] 删除的内容

Editor

▼ ←
▲
第 3 页: [2] 删除的内容

Editor

▼ ←
▲
第 3 页: [2] 删除的内容

Editor

▼ ←
▲
第 3 页: [2] 删除的内容

Editor

▼ ←
▲
第 3 页: [2] 删除的内容

Editor

▼ ←
▲
第 3 页: [2] 删除的内容

Editor

▼ ←
▲
第 3 页: [2] 删除的内容

Editor

▼ ←
▲
第 3 页: [2] 删除的内容

Editor

第 3 页: [2] 删除的内容 Editor

第 3 页: [2] 删除的内容 Editor

第 3 页: [2] 删除的内容 Editor

第 3 页: [2] 删除的内容 Editor

第 3 页: [2] 删除的内容 Editor

第 3 页: [2] 删除的内容 Editor

第 3 页: [2] 删除的内容 Editor

第 3 页: [2] 删除的内容 Editor

